



**HAL**  
open science

## Calibration of a super-Gaussian wake model with a focus on near-wake characteristics

Marie Cathelain, Frédéric Blondel, Pierre-Antoine Joulin, Pauline Bozonnet

### ► To cite this version:

Marie Cathelain, Frédéric Blondel, Pierre-Antoine Joulin, Pauline Bozonnet. Calibration of a super-Gaussian wake model with a focus on near-wake characteristics. *Journal of Physics: Conference Series*, 2020, Wind and Wind Farms, 1618 (6), pp.062008. 10.1088/1742-6596/1618/6/062008 . hal-02995695

**HAL Id: hal-02995695**

**<https://ifp.hal.science/hal-02995695>**

Submitted on 9 Nov 2020

**HAL** is a multi-disciplinary open access archive for the deposit and dissemination of scientific research documents, whether they are published or not. The documents may come from teaching and research institutions in France or abroad, or from public or private research centers.

L'archive ouverte pluridisciplinaire **HAL**, est destinée au dépôt et à la diffusion de documents scientifiques de niveau recherche, publiés ou non, émanant des établissements d'enseignement et de recherche français ou étrangers, des laboratoires publics ou privés.



Distributed under a Creative Commons Attribution 4.0 International License

PAPER • OPEN ACCESS

## Calibration of a super-Gaussian wake model with a focus on near-wake characteristics

To cite this article: M. Cathelain *et al* 2020 *J. Phys.: Conf. Ser.* **1618** 062008

View the [article online](#) for updates and enhancements.



**IOP | ebooks™**

Bringing together innovative digital publishing with leading authors from the global scientific community.

Start exploring the collection—download the first chapter of every title for free.

# Calibration of a super-Gaussian wake model with a focus on near-wake characteristics

M. Cathelain, F. Blondel, P.A. Joulin, P. Bozonnet

IFP Energies nouvelles, 1-4 avenue de Bois-Préau, 92852 Rueil-Malmaison, France

Email : marie.cathelain@ifpen.fr

**Abstract.** Offshore wind turbine near wakes can extend downstream up to  $5D$  due to low atmospheric turbulence intensities. They are characterised by strong velocity deficits, a transitioning Gaussian shape, and strong added turbulence intensities. Classical analytical wake models are still used due to their low computational costs, but they mainly focus on far-wake characteristics. A super-Gaussian wake model valid in near- and far-wake regions has recently been developed at IFP Energies nouvelles. This wake model requires calibration and validation. To this end, large-eddy simulations of the large DTU-10MW reference wind turbine under different neutrally stratified atmospheric flows are carried out with the LES Meso-NH model. A database is generated based on these results and used to calibrate and validate the super-Gaussian model.

## 1. Introduction

Estimation of wake losses is a critical part in a wind farm design process. Indeed, power losses due to wake effects are typically in the range of 10 to 20% and can rise up to 70% in the case of aligned turbines for wind velocities lower than the rated wind speed of the turbines [1]. Combining an accurate wake model to an optimisation algorithm results in a powerful tool, able to address the challenge of wind farm layout optimisation within a constrained area and the prediction of the annual energy production.

A wake is commonly characterised by a reduction of the wind speed and an increase of the turbulence intensity, but these properties can be investigated further: the wake is indeed defined by two regions, the near and the far wake. The near wake, in the vicinity of the turbine, has features that are directly related to the rotor geometry, its aerodynamics, and the inflow conditions. It is characterised by strong velocity deficits, a transitioning top-hat/Gaussian shape, and strong added turbulence intensities. The near-wake shape may be altered by the presence of the hub and tower wakes. The far wake is more influenced by the surrounding flow: turbulent mixing governs the wake recovery. The transition is often considered to be located around 3 to 4 turbine diameters  $D$ , but it actually depends on the atmospheric flow. For example, offshore turbine near wakes can extend up to  $5D$  due to lower atmospheric turbulence intensities. Geographical constraints (e.g. due to zoning regulation, water depth or soil conditions) can lead to wind farms with closely-spaced wind turbines (e.g.  $3.3D$  and  $4.2D$  minimal inter-distances respectively for Lillgrund and Ormonde offshore wind farms instead of 6 to  $8D$  for most offshore wind farms in the last decades). Under these conditions, wind turbines can operate in the near wake of upstream turbines. It is therefore necessary to accurately model near wake behaviour.



Several analytical models have been derived over the years, from the well-known Park model [2] and modified Park model [3] to the most recent models proposed by Frandsen et al. [4] or Bastankhah and Porté-Agel [5]. Most of commercial wind farm design software are based on analytical models due to their low computational costs. While these models mainly focus on far-wake characteristics, it seems necessary to develop engineering models that are valid in both near and far wake. To this end, a super-Gaussian wake model has been proposed [6] and requires further calibration and validation. The paper is organised as follows: in a first part, the super-Gaussian model is introduced with a focus on parameters to be calibrated. Then the meteorological LES solver Meso-NH and its recently implemented actuator line method [7] is presented, as well as the workflow adopted to generate the calibration database. Eleven simulations with different wind speeds and turbulence intensities are carried out with the DTU 10-MW wind turbine. Thrust and probe lines in the wake are extracted from the simulations and used for the calibration phase. Lastly, results are presented and discussed.

## 2. Super-Gaussian wake model

The derivation of the super-Gaussian model is based on the same principle as the model of Bastankhah and Porté-Agel [5], i.e. both mass and momentum are conserved. This differs from the work of Shapiro et al. [8], who originally suggested to use a super-Gaussian shape function. In their work, only mass conservation is enforced.

In the wake, the dimensionless velocity deficit is expressed as the product of the maximum velocity deficit  $C(\tilde{x})$  and a shape function  $f(\tilde{r})$ :

$$\frac{U_\infty - U_w}{U_\infty} = C(\tilde{x}) \times f(\tilde{r}) = C(\tilde{x}) \times e^{-\tilde{r}^n / (2\tilde{\sigma}^2)} \quad (1)$$

with  $U_\infty$  the wind velocity at infinity,  $U_w$  the velocity in the wake, and  $\tilde{x}$ ,  $\tilde{r}$  and  $\tilde{\sigma}$  respectively the axial distance from the turbine, the radial distance from the wake centre and a characteristic wake width that is the standard deviation when  $n = 2$ . The tilde symbol denotes a normalisation by  $D$ , the turbine diameter. The main difference with the Gaussian model is the shape function  $f(\tilde{r})$ , which is a super-Gaussian function with a radial distance to the power  $n$  and a squared characteristic wake width  $\tilde{\sigma}$ . An emphasis is given to the dependence on  $\tilde{x}$  to  $\tilde{\sigma}(\tilde{x})$  and  $n(\tilde{x})$ , but this notation is omitted for sake of simplification.

Typical super-Gaussian profiles are shown in Figure 1. The super-Gaussian is a convenient choice for representing wakes since for high values of the super-Gaussian order  $n$ , the function is close to a top-hat (as observed in the near wake) while for lower values of  $n$ , the function smoothly evolves towards the well-known Gaussian shape, as observed in the far wake (for  $n = 2$ , the super-Gaussian function is actually a Gaussian function). Depending on the value of the characteristic wake width  $\tilde{\sigma}$ , the wake width at the base can be slightly larger or thinner compared with the Gaussian counterpart ( $n = 2$ ). The highest value of characteristic wake width ( $\tilde{\sigma} = 0.6$ ), for which the wake base is thinner with the super-Gaussian model, is typical of far wake and high turbulence conditions. This case is not likely to occur as a Gaussian shape is expected in the far wake.

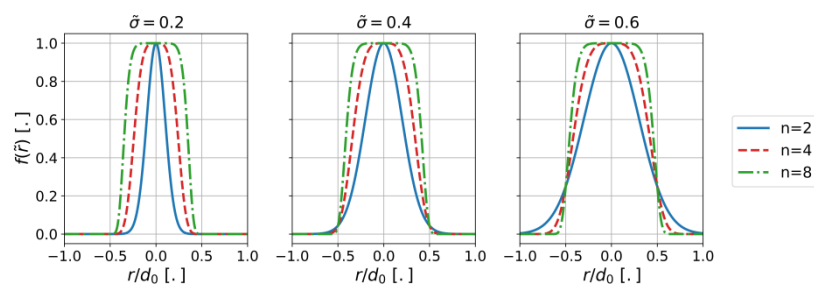


**Figure 1.** Super-Gaussian profiles of order  $n \in [2, 4, 8]$  for three different characteristic wake width values.

An expression for the maximum normalised velocity deficit  $C(\tilde{x})$  is derived in Blondel and Cathelain [6]:

$$C(\tilde{x}) = 2^{2/n-1} - \sqrt{2^{4/n-2} - \frac{nC_T}{16\Gamma(2/n)\tilde{\sigma}^{4/n}}}, \quad (2)$$

with  $\Gamma$  the Gamma function. The original form of  $C(\tilde{x})$  from Bastankhah and Porté-Agel is recovered when setting  $n$  to 2 [5].

In order to calibrate the super-Gaussian model, the variables  $n$  and  $\tilde{\sigma}$  need to be fitted. Two expressions are detailed in Blondel and Cathelain [6]:

$$\begin{cases} \tilde{\sigma} = (a_s TI + b_s)\tilde{x} + c_s\sqrt{\beta} \\ n = a_f e^{b_f \tilde{x}} + c_f \end{cases} \quad \text{with } \beta = \frac{1}{2} \times \frac{1 + \sqrt{1 - C_T}}{\sqrt{1 - C_T}} \quad (3)$$

with the characteristic wake width  $\tilde{\sigma}$  depending on the axial distance  $\tilde{x}$ , the turbulence intensity  $TI$  and the thrust coefficient  $C_T$  (through the expression of  $\beta$ ), and the evolution of super-Gaussian order  $n$  against the downwind distance following an exponential curve. In Blondel and Cathelain [6],  $a_s$ ,  $b_s$ ,  $c_s$  and  $a_f$ ,  $b_f$ ,  $c_f$  are kept constant in a first approach in order to keep a simple form of the model and to have a limited number of parameters to tune. A first calibration has been presented in [6], the values are recalled in Table 1. These results have been obtained based on two experimental campaigns [9] [10].

**Table 1.** Original fitted parameters.

$a_s$	$b_s$	$c_s$	$a_f$	$b_f$	$c_f$
0.17	0.005	0.20	3.11	-0.68	2.41

In order to extend the calibration database and to improve the robustness of the model, additional cases from numerical simulations are presented in the next section, involving a large wind turbine, different thrust coefficients and turbulence intensities.

### 3. Database generation using high-fidelity large-eddy simulations (LES)

#### 3.1. Meso-NH solver

Meso-NH is an open-source non-hydrostatic mesoscale atmospheric model developed by the Centre National de Recherches Météorologiques (CNRM - Météo France/CNRS) and the Laboratoire d'Aérodynamique (LA - UPS/CNRS) [11]. This LES model has recently been extended to wind farm flow simulations, using an Actuator Line Model (ALM) of the wind turbines [7]. It enables to simulate the interactions between wind turbines and surrounding atmospheric flows from meso- to micro-scales. A realistic atmosphere can be simulated with this model, including roughness effects, thermal effects, complex terrains, or even complex micro-physical phenomena.

#### 3.2. Simulation setup

**3.2.1. Precursor simulation.** The first phase of the simulation consists in generating an atmospheric state with controlled wind velocity and wind direction at the hub height. In this work, ideal cases are modelled with Meso-NH, meaning that cyclic conditions and ideal constant large-scale forcings are prescribed (i.e. there is no coupling with external numerical weather prediction models as the objective is to generate specific wind conditions). Moreover, the considered atmospheric boundary layer (ABL) is neutrally stratified with a constant vertical virtual potential temperature capped by a strong inversion layer at an altitude of 1 km. There is no orography and the surface roughness is uniform throughout the domain. The size of the father domain is 27 km  $\times$  2 km  $\times$  2 km with a 50 m grid resolution in horizontal directions and 2.5 m in vertical direction up to an altitude of 230 m with a constant stretching above. This small vertical resolution near the ground is required because the vertical grid

cannot be refined afterwards in Meso-NH (i.e. when the turbine is introduced in the domain after the precursor phase, the nested domains are refined in horizontal directions only). This vertical resolution is thus chosen so that the criterion of 30 to 60 cells per blade in the final mesh surrounding the turbine is respected [12].

This initial phase – a precursor simulation – is critical as the input parameters of the atmospheric model are the initial and geophysical fields (a radio sounding describing the vertical profiles of wind and potential temperature, idealised surface fluxes and global forcing fields), and not a prescribed wind at a specific height. The geostrophic wind prescribed as global forcing represents a uniform lateral pressure force which enables to maintain the large-scale wind above the ABL. In the ABL, the wind tends to slow down and rotate due to the friction with the surface, the pressure and the Coriolis force: it results in an Ekman layer. Close to the surface, an equilibrium is reached with the surface roughness and the wind profile tends towards a logarithmic law in the case of a neutral atmosphere. Initial fields and their evolution in time are shown in Figure 2. The vertical wind profile is similar to a logarithmic law near the surface as expected and a wind jet appears below the capping layer (typical of the Ekman layer, c.f. Eq 6.4.6c [13]).

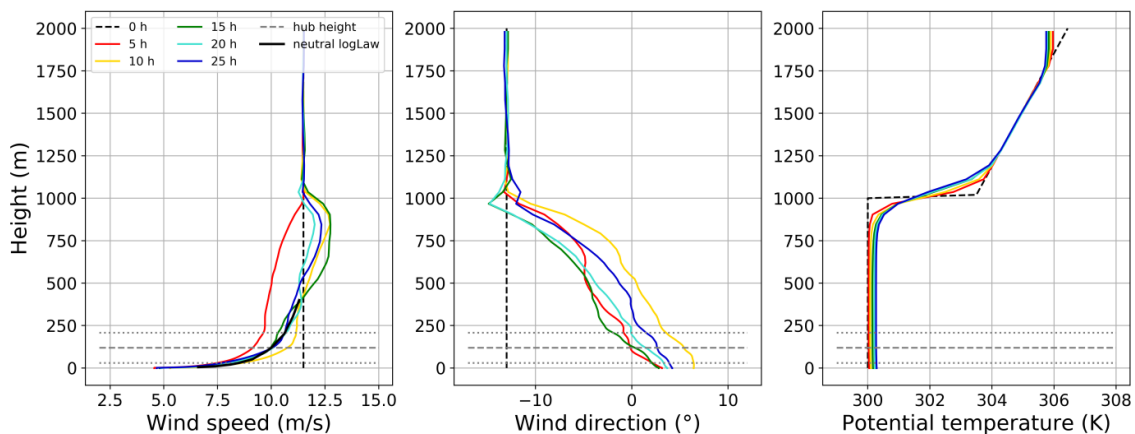


**Figure 2.** Evolution of vertical profiles of horizontal wind speed (left), wind direction (centre) and virtual temperature (right) for the precursor simulation.

The simulation runs until a quasi-steady-state ABL is obtained. In the literature, equilibrium times for neutral ABL are reported to be between 16 and 24 hours [14]. Figure 3 shows the evolution of the 10-minute average wind speed and direction at hub height: besides the variation of mean speed and direction over time, slight low-frequency oscillations are observed after a transient period (from 10h). These are inertial oscillations due to the Coriolis force whose period is  $2\pi/f_c \sim 16\text{h}$  (with  $f_c$  the Coriolis parameter such as  $f_c = 2\Omega \sin \varphi$  and  $\Omega$  the Earth rotation rate) under European latitudes (here  $\varphi = 49^\circ$ ). Since it was not possible to get rid of the inertial oscillations, the restart time for the simulation including the wind turbine is chosen in order to ensure a direction close to  $0^\circ$  during 1 h. Once the restart time is selected (here after 16h) and the wind conditions are known at hub height, the turbine is included into the domain using the actuator line method (ALM).

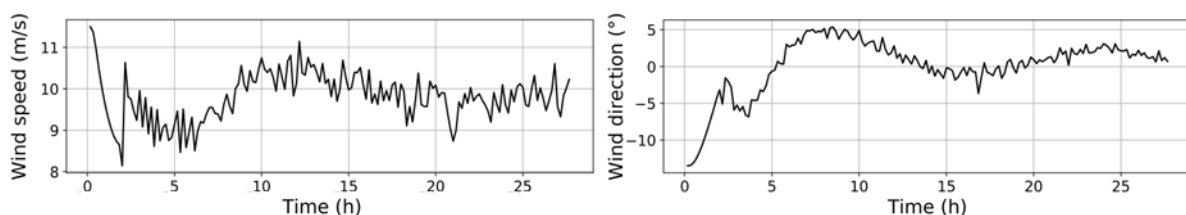


**Figure 3.** Evolution of 10-minute average horizontal wind speed (left) and wind direction (right) for the precursor simulation at hub height.

3.2.2. *Case setup.* The turbine considered in this work is the DTU 10-MW reference wind turbine (178.3 m-diameter and 119 m-hub height) [15]. Two mesh refinements (along horizontal directions) are introduced in the father domain so that the grid resolution around the turbine tends to 2.5 m (i.e.  $D/70$ ). Characteristics of the domains are given in Table 2. Because of the large cell size ratio between meshes, a distance of 2 km is imposed between Domain 2 and Domain 3 in order to let the turbulence from the father domain enters Domain 2 and breaks into smaller eddies before entering Domain 3. The cyclic boundaries of the father domain are maintained which explains the length of the domain (i.e. to avoid disturbance of the turbine by its own wake re-entering the domain). Two-way interactions are enabled between domains.

**Table 2.** Horizontal characteristics of the domains.

Domain	Horizontal resolution	$L_x \times L_y$	$N_x \times N_y$	Total number of cells
<b>Domain 1</b>	50 m $\times$ 50 m	151D $\times$ 11D	540 $\times$ 40	3 $\times$ 10 <sup>6</sup>
<b>Domain 2</b>	10 m $\times$ 10 m	50D $\times$ 6.7D	900 $\times$ 120	15 $\times$ 10 <sup>6</sup>
<b>Domain 3</b>	2.5 m $\times$ 2.5 m	30D $\times$ 4.5D	2160 $\times$ 324	98 $\times$ 10 <sup>6</sup>

The turbine is located at 15D behind the inlet of Domain 3 following the same principle as the one between Domain 2 and Domain 3 on turbulence establishment. The behaviour of the turbulence breaking into smaller scales can be observed in Figure 4 in Domain 3: over a distance of 1 to 2 km from the inlet, eddies are large and diffuse before breaking down into smaller structures.

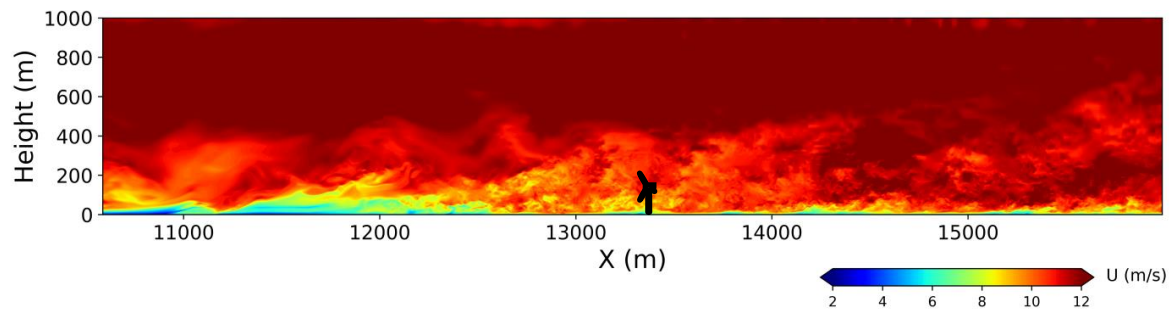


**Figure 4.** Instantaneous horizontal velocity at mid domain of Domain 3 (without wind turbine).

The turbine is modelled using the ALM but neither the hub nor the nacelle are modelled. No bending, precone and tilt are taken into account. The controller has not been implemented yet, hence the operating conditions (i.e. rotational speed and pitch) are imposed each 10-minute period by interpolating into the steady state operational data table of the INNWIND benchmark [16]. The interpolation is based on the wind conditions calculated from the previous 10-minute period. The first 10-minute period is not useable as the wake starts to develop.

Different geostrophic winds and three values of roughness length ( $z_0 = 0.0002$  m, 0.01 m and 0.7 m representing respectively offshore, open flat onshore and very rough onshore surfaces [17]) are imposed, leading to eleven cases with different wind speeds at hub height and different turbulence intensities (TI). A summary of these cases can be found in Table 3.

**Table 3.** Characteristics of geostrophic wind and wind at hub height.

	Case 1	Case2	Case 3	Case 4	Case 5	Case 6	Case 6	Case 7	Case 7	Case 8	Case 9
Geo. wind (m/s)	7.5	8.5	9.5	10.5	11.5	12.5	12.5	15.5	15.5	17.5	10.5
Wind speed (m/s)	6.6	7.1-7.8	8.5	9.4-9.8	9.6-10.2	10.6	11.6-11.8	12.8	14.0	15.8	7.9
TI (%)	9.4	9.3-10.7	9.5	9.4-10.3	10.1	9.7	5.6-6.9	10.2	7.4	7.0	14.0
$z_0$ (m)	0.01	0.01	0.01	0.01	0.01	0.01	0.0002	0.01	0.0002	0.0002	0.7

An example of 10-minute average horizontal wind field and turbulence intensity for case 4 is shown in Figure 5. One can notice the wake development behind the turbine with a non-realistic acceleration of the flow in the centre of the near wake: this is due to the absence of the hub which creates a Venturi effect up to  $1-2 D$ . For each case and each 10-minute segment, the 3D wind field is saved along transverse probe lines at hub height from  $X = 1D$  to  $10D$  behind the turbine. These data are then used to calibrate the super-Gaussian model in the following section.

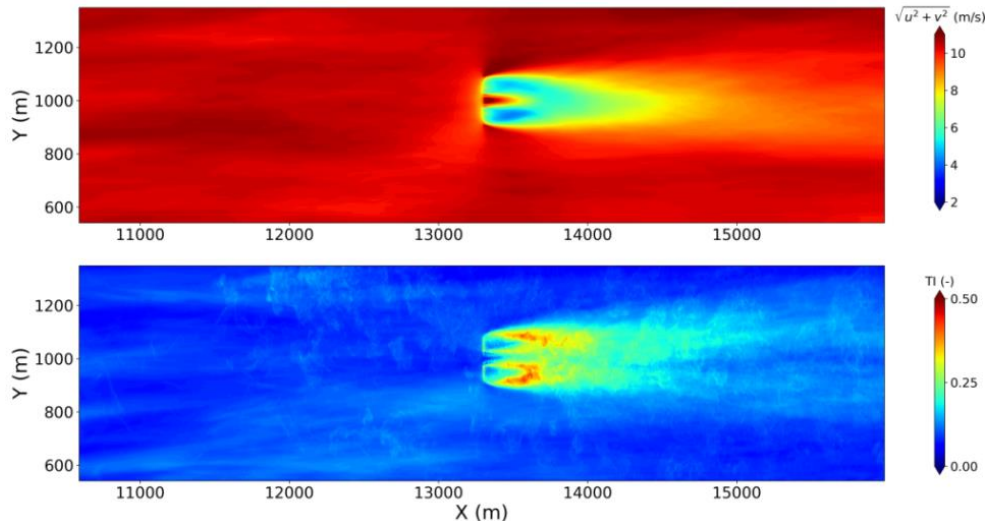


**Figure 5.** Horizontal plane of 10-minute average horizontal wind field (top) and turbulence intensity (bottom) at hub height for case 4 (mean wind speed: 10.2 m/s, mean ambient TI: 0.103).

10-minute average power and thrust of the turbine are shown in Figure 6: these results can slightly differ from results obtained with other codes (e.g. HAWC2 and EllipSys3D in [16]). Indeed, the operating conditions (blade pitch, rotational speed) may differ here from the original behaviour of the turbine: they are interpolated based on the computation of the mean wind speed over a line which has the extension of the rotor at  $X = -2.5D$  from the previous 10-minute segment (T-1) and this 10-minute average wind speed is subject to small variations as shown in Figure 3. Regarding the large variations of thrust and power at high wind speeds in Figure 6, the above-mentioned strategy is limited. Indeed, a small difference in the 10-minute average inflow wind speed at T-1 compared to the actual wind speed at segment T leads to a large difference on the operating blade pitch angle, and has a large impact on power and thrust at such high wind speeds. The implementation of a real-time controller is ongoing. It is emphasized that the same turbine behaviour is modelled in the super-Gaussian wake model: the thrust coefficient  $C_T$  is calculated using variables from the LES, such as thrust, density, and upstream wind velocity at  $X = -2.5D$  and is then used in the calibration phase of the super-Gaussian model in the following section.

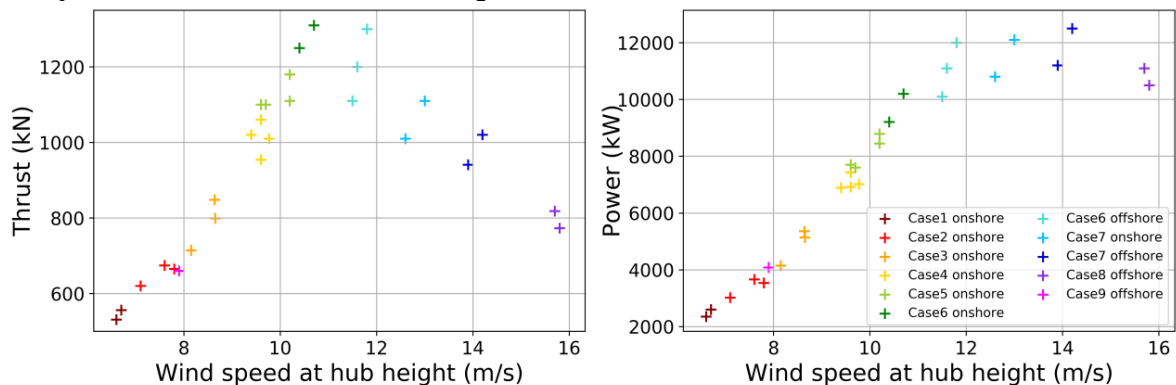


**Figure 6.** Thrust and power curve from 10-minute average results from Meso-NH-ALM.

## 4. Calibration and validation results

### 4.1. Calibration procedure

The aforementioned LES database is used to calibrate the super-Gaussian wake model. It covers a large range of wind speeds (6.6 to 15.8 m/s), thrust coefficients (0.21 to 0.86), and three values of surface roughness ( $z_0 = 0.0002$  m, 0.01 m and 0.7 m). The hypothesis mentioned in [6] about the constant parameters of the analytical wake model does not hold anymore. Indeed, a dependence on the thrust coefficient and the turbulence intensity seems to be required in order to have a better representation of the wake in both near- and far-wake regions.

Concerning the characteristic wake width  $\tilde{\sigma}$  in Equation (3), the parameters of the growth rate (i.e.  $a_s$  and  $b_s$ ) remain constant but the coefficient  $c_s$  becomes a linear function of the thrust coefficient. This dependence has been observed in the analysis of the LES simulation results:

$$c_s = c_{s_1} \times C_T + c_{s_2}. \quad (4)$$

Concerning the super-Gaussian order  $n$  in Equation (3), a dependence on the turbulence intensity is introduced with:

$$b_f = n_{b_{f_1}} \exp(-n_{b_{f_2}} \times TI) - n_{b_{f_3}}. \quad (5)$$

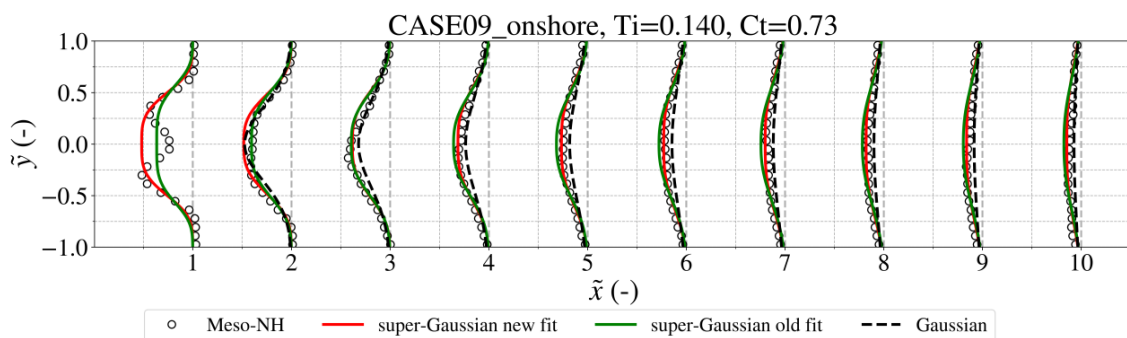
With this parameterisation, the rate of decrease of  $n$  is lowered at low turbulence intensities accounting for lower turbulent mixing of the wake under these conditions. The maximum value of the super-Gaussian order is set in order to respect the actuator-disk theory: the velocity at the disk should be equal to  $U_{\text{disk}} = U_\infty(1 - a)$  with  $a$  the axial induction factor calculated from the thrust coefficient ( $a = 1/2(1 - \sqrt{1 - C_T})$ ). At the disk, the maximum normalised velocity deficit  $C(0)$  equals  $a$ :  $a_f$  thus ensures that this boundary condition at the rotor is satisfied. The parameter  $c_f$  remains constant. From the analysis of the LES simulations, it appears that  $c_f$  is not equal to 2: the Gaussian shape is not fully recovered, even in the far wake.

The new set of parameters that can be tuned are summarised in Table 4. The optimisation problem is solved using the differential evolution algorithm provided in SciPy library (with a larger weight on the error in the near wake than in the far wake for the computation of the global error) leading to the following values for the parameters:

**Table 4.** New fitted parameters.

$a_s$	$b_s$	$c_s$	$a_f$	$b_f$	$c_f$
0.18	0.0119	$0.0564 \times C_T + 0.13$	Ensures $C(0) = a$	$1.59 \times \exp(-23.31 \times TI) - 2.15$	2.98

The velocity deficits in the wake at distances from  $\tilde{x} = 1$  to 10 behind the turbine are shown in Figure 7 for both Meso-NH simulations and super-Gaussian model with the old and new fitted parameters, and classical Gaussian model [5]. The Gaussian model is used in the following figures with  $k_a = 0.38$ ,  $k_b = 0.003678$  and  $\varepsilon = 0.2\sqrt{\beta}$ .



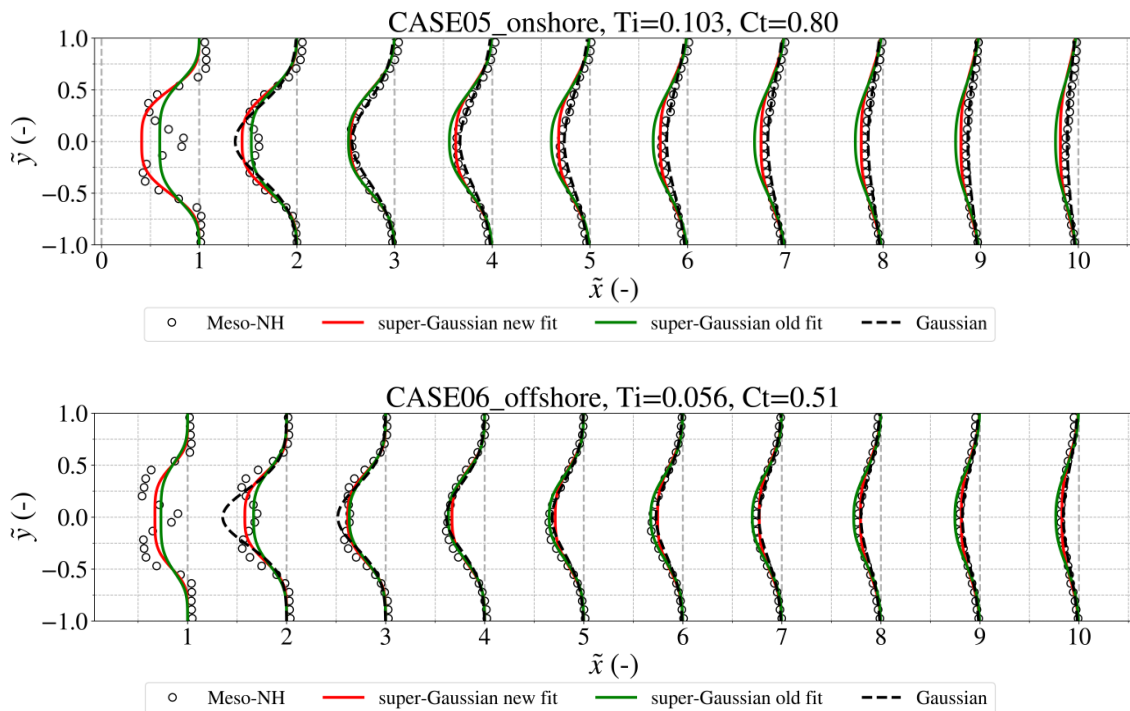


**Figure 7.** Normalised velocity deficit at ten axial distances behind the turbine.

One can note that the shape of the LES measurements in the near wake is due to the absence of hub in the actuator line modelling. For the high turbulence cases ( $TI \sim 0.14$  and  $0.10$ ), the new set of parameters improves significantly the shape and the maximum velocity deficit in the near wake compared to the old set. The behaviour in the transition ( $\tilde{x} = 2$  to  $3$ ) and in the far wake is properly captured in both regions. The maximum velocity deficit for the low turbulence case ( $TI = 0.056$ ) still needs some improvement in the near wake, however the probability of two turbines being located at a distance smaller than  $2D$  is very poor.

#### 4.2. Validation cases

Once the super-Gaussian has been calibrated on the LES dataset, a series of validation tests is carried out on experimental datasets.

*4.2.1. Model scale wind turbine.* The wake model is compared to wind tunnel measurements performed in the wake of a model scale wind turbine immersed in two neutrally-stratified turbulent boundary layers [18]. This study focused on the wake width, the velocity deficit, and the Reynolds stress in the far wake region. The high turbulence case ( $TI = 0.15$ ) is shown in Figure 8. For more quantitative comparisons, the root mean square error (RMSE) is computed at each distance where measurements are available. The newly calibrated super-Gaussian model brings a significant improvement in the near wake.

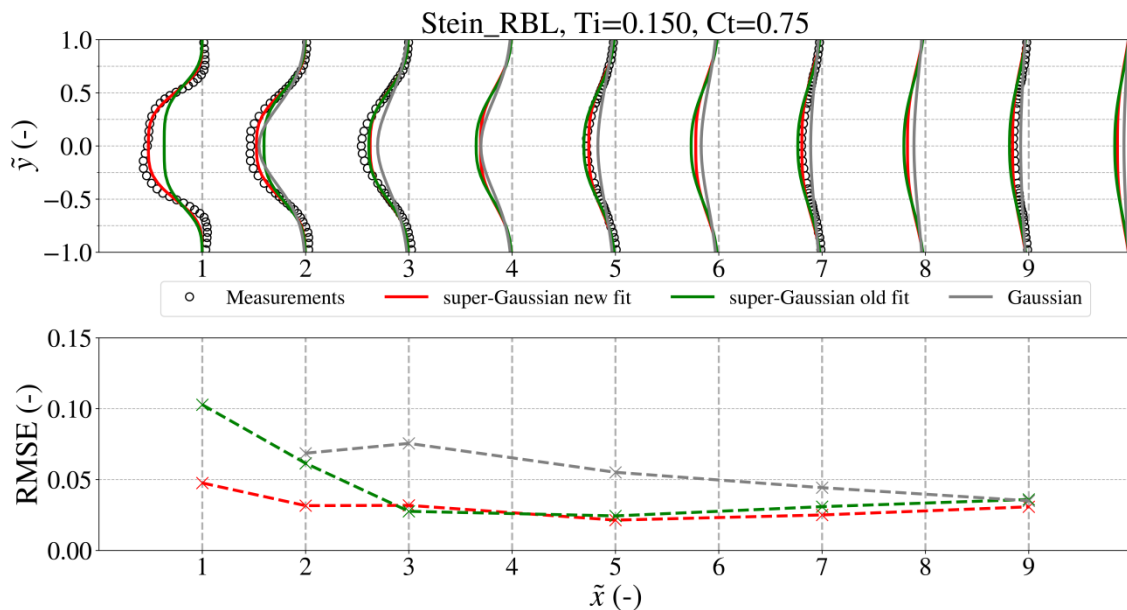


**Figure 8.** Normalised velocity deficit at ten axial distances behind the turbine (top) and corresponding RMSE (bottom) (measurements are provided by Stein [18]).

A second wind tunnel experiment [19] is used in this validation work. Hub-height horizontal plane Particle Image Velocimetry measurements of the wake behind a yawed wind turbine are compared in Figure 9: only the case with the non-yawed turbine is shown, the validation of misaligned wakes is part of a complementary work.

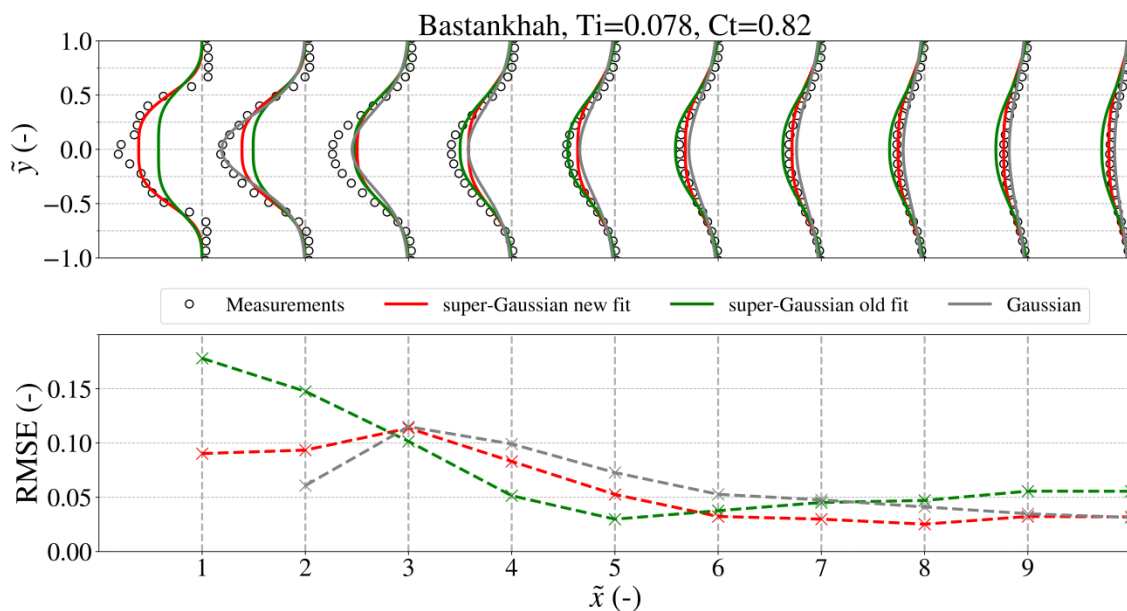


**Figure 9.** Normalised velocity deficit at ten axial distances behind the turbine (top) and corresponding RMSE (bottom) (measurements are extracted from [19]).

As in the previous case, the new fitted parameters bring a significant improvement in the near wake, except at  $\tilde{x} = 2$  compared to the Gaussian model. However, for this specific case, the maximum velocity deficit is slightly underestimated at  $\tilde{x} = 3, 4$  and  $5$  compared to the super-Gaussian model with the old fit. A slight improvement is observed in the far wake.

4.2.2. *The SWiFT benchmark.* The super-Gaussian wake model is compared to the LiDAR measurements and LES SOWFA results from the SWiFT benchmark, part of the IEA Wind Task 31 Wakebench group [10]. A small wind turbine (i.e. 27 m-diameter and 32.1 m-hub height) has been equipped with a scanning LiDAR and CFD and engineering models from the wind energy community have been compared to the LiDAR measurements in neutral, stable and unstable conditions. Only the neutral case is considered in Figure 10. One can note that the LiDAR measurements have been re-centred around  $\tilde{y} = 0$  as a small shift is observed in the original data.

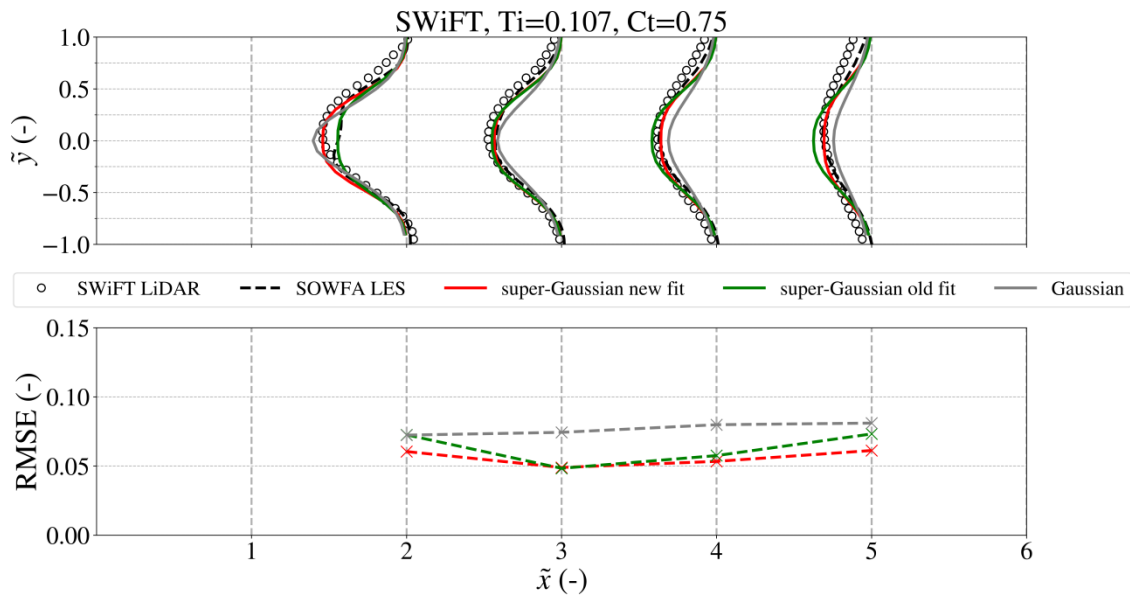


**Figure 10.** Normalised velocity deficit at four axial distances behind the turbine (top) and corresponding RMSE (bottom) (measurements in dots are extracted from [10]).

The new set of parameters for the super-Gaussian leads to a better prediction of the maximum velocity deficit in the near wake.

## 5. Conclusions

The workflow introduced in this work aims at providing an extensive dataset based on large-eddy simulations of a large wind turbine. This wind turbine modelled with the actuator line method is placed in a neutral atmospheric boundary layer simulated with Meso-NH, an open-source non-hydrostatic mesoscale atmospheric model [7]. The study provides detailed explanations on the generation of a realistic atmospheric flow with an appropriate modelling of the turbulence near the turbine. This process ends up in eleven simulations covering a large range of wind speeds (6.6 to 15.8 m/s), thrust coefficients (0.21 to 0.86), and three values of surface roughness ( $z_0 = 0.0002$  m, 0.01 m and 0.7 m) leading to turbulence intensity levels from 5.6% up to 14.0%.

This extensive dataset is then used to calibrate a super-Gaussian wake model [6]. A new parameterisation of the super-Gaussian order and the characteristic wake width is introduced with parameters depending on the turbulence intensity and on the thrust coefficient, while most of the parameters were set constant in a first study. This new set of parameters is optimised using the LES dataset through a differential evolution algorithm. The new super-Gaussian wake model is then compared to LiDAR field measurements and wind tunnel measurements: a significant improvement is observed in the near wake, whereas the results are slightly improved in the far wake. The impact of the hub modelling on the near-wake properties in the LES results requires a comprehensive study in the future. Additional simulations based on high thrust coefficients and low turbulence levels and respectively low thrust coefficients and high turbulence levels should also be considered.

**References**

- [1] Barthelmie R *et al* 2009 *Wind Energy* **12**
- [2] Jensen N 1983 Technical report from the Riso National Laboratory (Riso-M-2411)
- [3] Katic I, Hojstrup J and Jensen N 1986 *Proc. European Wind Energy Association Conference & Exhibition*
- [4] Frandsen S *et al* 2006 *Wind Energy* **9**
- [5] Bastankhah M and Porté-Agel F 2014 *Wind Energy* **70**
- [6] Blondel F and Cathelain M 2020 *Wind Energ. Sci. Discuss.* (in review)
- [7] Joulin P *et al* 2020 *Frontiers* **7**
- [8] Shapiro C, Starke G, Meneveau C and Gayme D 2019 *Energies* **12**
- [9] Aubrun S, Loyer S, Hancock P and Hayden P 2013 *J. Wind Eng. Ind. Aerod.* **120**
- [10] Doubrawa P *et al* 2020 *Wind Energ. Sci. Discuss.* (in review)
- [11] Lac C *et al* 2018 *Geosci. Model Dev.* **11**
- [12] Jha P, Churchfield M, Moriarty P and Schmitz S 2014 *J. Sol. Energy Eng.* **136**
- [13] Stull R 1988 An introduction to boundary layer meteorology
- [14] Allaerts D and Meyers J 2017 *J. Fluid Mech.* **814**
- [15] Bak C *et al* 2013 The DTU 10-MW Reference Wind Turbine, Sound/Visual production (digital)
- [16] Lekou D *et al* 2013 INNWIND project: Contribution to the Deliverable 2.21
- [17] Burton T *et al* 2001 *Wind Energy Handbook*. West Sussex: John Wiley & Sons, Ltd
- [18] Stein V and Kaltenbach H 2019 *Energies* **12**
- [19] Bastankhah M and Porté-Agel F 2016 *J. of Fluid Mech.* **806**